Sgs1^{BLM} independent role of Dna2^{DNA2} nuclease at DNA double strand break is inhibited by Nej1^{XLF}

Aditya Mojumdar, Nancy Adam, and Jennifer A. Cobb*

Departments of Biochemistry & Molecular Biology and Oncology, Robson DNA Science Centre, Arnie Charbonneau Cancer Institute, Cumming School of Medicine; University of Calgary; 3330 Hospital Drive N.W., Calgary, AB T2N 4N1, Canada.

* Lead Contact: Tel.: +1 403 220 8580 or Email: jcobb@ucalgary.ca

Short Title: Interplay of Nej1-Dna2 nuclease at DSB

Keywords: DSB repair, Repair pathway choice, Nej1, Sae2, Dna2, 5' resection, end-bridging

ABSTRACT

The two major pathways of DNA double strand break (DSB) repair, non-homologous end-joining (NHEJ) and homologous recombination (HR), are highly conserved from yeast to mammals. Regulated 5' DNA end resection is important for repair pathway choice and repair outcomes. Nej1 was first identified as a canonical NHEJ factor involved in stimulating the ligation of broken DNA ends and, more recently, it was shown to be important for DNA end-bridging and inhibiting Dna2-Sgs1 mediated 5' resection. Dna2 localizes to DSBs in the absence of Sgs1 through interactions with Mre11 and Sae2 and DNA damage sensitivity is greater in cells lacking Dna2 nuclease activity compared to *sgs1*Δ mutants. Dna2-Sae2 mediated 5' resection is down-regulated by Nej1, which itself interacts with Sae2. The resection defect of *sae2*Δ and the synthetic lethality of *sae2*Δ *sgs1*Δ are reversed by deletion of *NEJ1* and dependent on Dna2 nuclease activity. Our work demonstrates the importance of Nej1 in inhibiting short-range resection at a DSB by Dna2-Sae2, a critical regulatory mechanism that prevents the formation of genomic deletions at the break site.

AUTHOR SUMMARY

Nej1 regulates double-strand break (DSB) repair pathway choice through the inhibition of 5' DNA resection. Nej1 not only inhibits resection mediated by Dna2-Sgs1, but it inhibits Dna2 localization to the DSB through Sgs1-independent mechanisms involving Sae2 and Mre11. Nej1 interactions with Sae2 promote genome stability by inhibiting the initiation 5' DNA resection by Sae2-Dna2.

INTRODUCTION

DNA double-strand breaks (DSBs) can be repaired by two central pathways, non-homologous end joining (NHEJ) and homologous recombination (HR). NHEJ mediates the direct ligation of DNA ends without the requirement for end processing, whereas HR requires 5' end resection. Both the initiation of resection and end-bridging at a DSB are important for repair pathway choice and down-stream processing. Once resection initiates at a DSB, repair by canonical NHEJ is no longer an option. Therefore, a complex network of proteins has evolved to regulate this key step, which by extension governs repair pathway choice.

yKu70/80 (Ku) and Mre11-Rad50-Xrs2 (MRX) are the first complexes that localize to a DSB and both are important for recruiting the NHEJ factor, Nej1 [1-4]. Cells lacking *NEJ1* are as defective in end-joining as *ku70*Δ and *dnl4*Δ [3, 5, 6]. After localization, Nej1 stabilizes Ku, which protects the DNA ends from nucleolytic degradation, and promotes Lif1-Dnl4 mediated ligation [2, 3, 7, 8]. Nej1 also inhibits Sgs1-dependent 5' DNA resection through a mechanism in which Nej1 binds to both Mre11 and Sgs1, inhibiting Dna2 localization [4, 9]. While Nej1 functions antagonistically to MRX in the context of 5' resection, Nej1 aligns with MRX functionality in DNA end-bridging. The structural features of the MRX complex are critical for end-bridging, and bridging defects associated with *NEJ1* deletion are additive with a *rad50* mutant that is proficient in resection, but defective in end-bridging [4, 10-13].

Sae2, the yeast homologue of human CtIP, interacts with the MRX-complex and initiates resection by activating Mre11 3' to 5' endonuclease which results in Ku dissociation from the DNA ends [14, 15]. After resection initiates by Sae2-dependent Mre11 activation, long-range resection proceeds from two functionally redundant 5' to 3' nucleases, Dna2 in complex with Sgs1 helicase or Exo1 [15, 16]. Dna2 is mutated in a myriad of human cancers but understanding its entire function at DSBs has been challenging because *DNA2* is an essential gene involved in Okazaki fragment processing, therefore it cannot be deleted [17-21]. The lethality of *dna2*Δ is supressed by disruption of *PIF1* helicase [22]. Dna2 has both 3' to 5' and 5' to 3' endo/exonuclease activity and 3' to 5' helicase activity. It is an inefficient helicase, thus Sgs1 provides this activity during long-range resection [17, 23, 24]. Dna2 is recovered at a HO-

induced DSB and resection defects at the break in *dna2*Δ *pif1*-m2 isogenic cells were equivalent +/-*SGS1* [16]. This epistatic relationship for *DNA2* and *SGS1* provided support to the model that Dna2-Sgs1 function as complex in DSB repair. However, these data do not account for the greater sensitivity of *dna2*-1 *sgs1*Δ to IR and UV compared to single mutants, with nuclease deficient *dna2*-1 (P504→S) showing greater sensitivity than *sgs1*Δ [25]. While Dna2 has an important role in 5' resection, there is currently a gap understanding its entire functionality and regulation at the DSB.

In the absence of Sae2 or Mre11 nuclease activity, resection initiates primarily through Dna2 activity, not through Exo1 [26-28]. However, the ability of these long-range nucleases to serve as compensatory back-ups and initiate resection largely depends on Ku binding. The DSB sensitivity and resection deficiency of *mre11*-nuclease dead mutants are alleviated by disrupting Ku. When DNA ends are exposed from the loss of Ku, they are rapidly recognized as substrate for Exo1 nuclease. This two-step model for the initiation and then long-range resection depends on different nucleases, however current data does not exclude a function for Dna2 in both. Like Mre11, Dna2 has 3' to 5' endonuclease activity and the nuclease activities of Dna2 and Mre11 show functional redundancy for processing the ends of DSBs after radiation treatment [24]. Moreover, when *NEJ1* is deleted and Dna2 levels increase, 5' resection increases similarly in wild type and nuclease-dead *mre11*-3 mutant cells. How Nej1 functions to down-regulate Dna2-dependent 5' resection remains obscure, but the mechanism is likely more intricate than simply blocking Dna2-Sgs1 interactions with Mre11 [4]. For example, Sae2 was recently shown to stimulate the nuclease and helicase activity of Dna2-Sgs1, although this needs to be demonstrated *in vivo* at the break site [29, 30]. The relationship between Nej1 and Sae2 warrants investigation for this reason and because like MRX and Nej1, Sae2 has a role in DNA end-bridging at DSBs [31], a function conserved in humans and with Ctp1 in fission yeast [32, 33].

Here we determine the implications of regulating Nej1 and Dna2 levels at a DSB in DNA processing and the physiological importance of Nej1-dependent inhibition of Dna2-Sae2 interaction. In nuclease deficient *dna2*-1 mutants, NHEJ mediated repair increases after DSB

formation as do the levels of Nej1 and Ku binding. We had previously shown the inverse, where Dna2 levels increase at DSBs in *nej1*Δ mutants. In the current work we find Nej1 interacts with Sae2 and down-regulated Sae2 binding to both MRX and Dna2. Deletion of both *NEJ1* and *SAE2* showed epistatic end-bridging defects, increased 5' resection, and the development of large deletions at the break site compared to *sae2*Δ single mutant cells. Lastly, we show that deletion of *NEJ1* can reverse the synthetic lethality of *sae2*Δ *sgs1*Δ through a mechanism dependent on the nuclease activity of Dna2.

RESULTS

Sgs1-independent recruitment of Dna2 nuclease is inhibited by Nej1 at DSB

Nej1 promotes NHEJ and down-regulates 5' DNA resection by inhibiting Sgs1-dependent recruitment of Dna2 to a DSB [4, 9]. Deletion of *SGS1* reverses hyper-resection and the large genomic deletions that form at a DSB break in *nej1*Δ mutants. To determine whether loss of Dna2 nuclease activity shows similar, we combined nuclease dead *dna2*-1 with *nej1*Δ [17, 18]. Resection was measured by quantitative PCR-based approach and relies on a *Rsa*I cut site 0.15kb from the DSB as previously described [9, 31]. *Rsa*I will be unable to cleave if resection has proceeded past the cut site as single-stranded DNA is present and the region can be amplified by PCR (Figure 1A). 5' resection was reduced more in *dna2*-1 compared to *sgs1*Δ mutants, and the rate in *dna2*-1 *nej1*Δ was far below wild type and *sgs1*Δ *nej1*Δ (Figure 1B). We performed chromatin immuno-precipitation (ChIP) at the HO-induced DSB and observed that Dna2 recruitment was similarly compromised in *sgs1*Δ and *dna2*-1 mutant cells (Figure 1C), however Sgs1 recruitment remained at wild type levels in *dna2*-1 (Figure S1A). Dna2 binding to Sgs1 is inhibited by Nej1 and consistent with previous reports, its recruitment to a DSB increases in *nej1Δ* and is reduced, but not gone, in *sgs1*Δ mutants (Figure 1C) [4, 9]. Strikingly, Dna2 can be recruited to a DSB independently of Sgs1 via a pathway that is also inhibited by Nej1 as its recovery in *sgs1*Δ *nej1*Δ was above wild type and similar to the level in *nej1*Δ mutants (Figure 1C).

The level and functionality of these factors at a DSB dramatically impacts repair pathway choice. We previously showed that overexpression of Dna2 resulted in decreased Nej1 recovered at the DSB [4]. Under conditions of Dna2 deficiency in cells harboring *dna2*-1, Nej1 recovery increased as did the rate of NHEJ repair (Figures S1B, 1D). By contrast, Nej1 levels were unaltered in *sgs1*Δ, which is notable given Nej1 physically interacts with Sgs1 but not Dna2 [4]. In *NEJ1*+ cells, end-joining as determined by survival on galactose inversely correlates with 5' DNA resection, increasing in *sgs1*Δ and even more so in *dna2*-1 mutants. As Nej1 is essential for NHEJ, growth on galactose was markedly reduced in all mutant combinations containing *nej1*Δ (Figure 1D).

Determining the mating type of survivors that grow on galactose provides a physiological readout of DNA processing events and genomic alterations occurring at a HO-induced DSB located within MATα1 and adjacent to MATα2 (Figure 1E). Expression of these genes regulate the mating type by activating alpha-type genes and inhibiting a-type genes. Extensive resection leads to large deletions (>700 bp) and disruption of both α1 and α2 genes, with a-like survivors (red), whereas small deletions or insertions lead to sterile type survivors (yellow). Repair events resulting in α-type survivors show no sequence change at the HO recognition site and usually develop from disruption in the HO endonuclease (gray). In WT cells and *sgs1*Δ mutants, the majority of survivors are sterile, and contain small insertions or deletions in the *MATα1* gene (Figure 1E) [9, 34]. By contrast, *dna2*-1 survivors were primarily MATα, indicating an increase in the rate of canonical NHEJ. The cut efficiency in *dna2*-1 mutants was similar to wild type 2 hours after galactose induction, however HO-cutting was completely abrogated in *dna2*-1 survivors (Table S4), which is consistent with canonical NHEJ repair and survivors having alterations in the endonuclease.

Dna2 recruitment to DSB is independent of Exo1

We next determined the involvement of the other nucleases, Mre11 and Exo1, in Dna2-mediated 5' resection at the DSB independently of Sgs1. MRX is important for the localization of many DSB processing factors including Nej1 and the long-range resecting factors, Exo1 and Dna2-Sgs1, which serve as back-ups to initiate resection. 5' resection in *mre11*-3 was similar to

wild type (Figure 2A) [9]. Resection in *exo1*Δ was also indistinguishable from wild type, however when combined with *sgs1*Δ, the level in *exo1*Δ *sgs1*Δ decreased more than in *mre11*-3 *sgs1*Δ mutants (Figures 2A, B). Upon deletion of *NEJ1*, resection in *mre11*-3 *sgs1*Δ *nej1*Δ was indistinguishable from wild type (Figure 2A), and partially restored in *exo1Δ sgs1*Δ *nej1*Δ mutants (Figure 2B). By contrast, the rates of 5' resection in *mre11*-3 *dna2*-1 and *exo1*Δ *dna2*-1 double mutants were severely reduced, and lower than double mutant combinations with *sgs1*Δ (Figures 2A, 2B and 1B). As with *dna2*-1 *nej1*Δ (Figure 1B), the deletion of *NEJ1* modestly rescued the low level of resection in *exo1*Δ *dna2*-1 cells, however the rate of resection was similarly reduced in *mre11*-3 *dna2*-1 and *mre11*-3 *dna2*-1 *nej1*Δ (Figures 2A, B).

As with wild type, *mre11*-3 and *exo1*Δ single mutant survivors had small indels (Figure 2C) and end-joining increased more when these mutations were combined with *dna2*-1 compared to double mutant combinations with *sgs1*Δ (Figure 2D). While overall survival decreased when *NEJ1* was deleted in combination with these double mutants (Figure 2D), the percentage of survivors with large deletions increased (Figures 2C, D). Survival was equally low in all mutant combinations with *nej1*Δ (Figure 2D), however survivors harboring *dna2*-1 showed an increase in non-mutagenic NHEJ, with fewer indels and no large deletion compared to triple mutant combinations with *sgs1*Δ (Figure 2C).

To determine whether 5' resection and HO survival differences in *mre11*-3 and *exo1*Δ were related to Dna2 localization +/- *SGS1* status, ChIP was performed on Dna2 in the different mutant combinations. Deletion of *NEJ1* increased the recovery level of Dna2 at the break in all mutant backgrounds (Figure 2E). Even though the rate of resection was lower in *exo1*Δ *sgs1*Δ mutants compared to *sgs1*Δ, the level of Dna2 recovered was similar (Figure 2E). Consistently, deletion of Exo1 did not alter 5' resection or Dna2 levels in otherwise wildtype or nej1Δ mutants (Figures 2B, 2E). By contrast, the recovery of Dna2 in *mre11*-3 sgs1Δ was higher than in *sgs1*Δ (p-value < 0.05), and similar to wild type (Figures 2E, 1C). Overall, these data suggest that Sgs1-independent recruitment of Dna2, which is inhibited by Nej1, involves a factor linked to Mre11 nuclease activity. This led us to investigate a potential role for Sae2, which was recently shown to increase at the DSB in *mre11*-3 mutants [27].

Sae2-dependent recruitment of Dna2 is inhibited by Nej1

Sae2 interacts with the MRX complex to activate Mre11 endonuclease and more recently it was also shown to stimulate the nuclease activity of Dna2 [15, 29, 30]. While Sae2 recruitment is abrogated in *mre11*Δ, levels increase in *mre11*-3 (Figure 3A) [27]. Thus, we determined whether the presence of Dna2 at the DSB in *mre11*-3 depended on Sae2. Indeed, the recruitment of $Dna2^{HA}$ significantly decreased in *mre11-3 sae2*Δ and *sae2*Δ (Figure 3B). As Nej1 inhibits Dna2, we next determined Dna2 recovery when *NEJ1* was deleted in combination with *sae2*Δ. Interestingly, Dna2 levels were lower in *sae2*Δ *nej1*Δ compared to *sgs1*Δ *nej1*Δ, which similar to *nej1*Δ (Figures 1C, 3B).

Underscoring the relationship between Dna2 and Sae2, increased recovery of Dna2 in *mre11*-3 *nej1*Δ double mutants was Sae2 dependent (Figures 2E and 3B). In the course of our investigation, we also observed that Sae2 levels increased in *nej1*Δ (Figure 3A), and the increase was additive in combination with *mre11*-3. Conversely, Sae2 recovery in *dna2*-1 remained indistinguishable from wild type as it did in *sgs1*Δ and *exo1*Δ mutants (Figures S1D, E). Thus, Nej1 appears regulate Sae2 levels as a way to inhibit resection at DSBs. When measured directly, we saw that hyper 5' resection in *nej1*Δ was reversed by deletion of *SAE2* (Figure 3C).

Similar to *dna2*-1, the rate of survival and non-mutagenic end-joining increased in *sae2Δ* mutants (Figure 3D). However, unlike *dna2*-1, large deletion developed when *sae2*Δ was combined with *nej1*Δ (Figures 1E, 3E). Previously, we showed that both 5' resection levels and DNA end-bridging defects contribute to the development of large deletions around a DSB [4]. End-bridging was measured using a strain with TetO at 3.2 Kb upstream and the LacO array at 5.2Kb downstream of the cut site. These cells express GFP-tagged TetR and mCherry-tagged LacO, enabling us to visualize the two sides of the break site by fluorescence microscopy (Figure 3F). In asynchronous cells, the distance between the GFP and mCherry foci was measured prior to (0 hr) and after (2 hr) DSB induction. Wild-type cells did not have a significantly different mean distance (0.24 and 0.28µm respectively), indicative of successful DNA end-bridging.

End-bridging was defective in *sae2Δ*, but not in *dna2*-1 mutant cells (Figures 3F, S2). Comparing *mre11*-3 and *sae2*Δ +/- *NEJ1* in 5' resection and end-bridging provides support for a model

where both processes safeguard against the development of large deletions. In *mre11*-3 mutants, resection proceeds but end-bridging is not disrupted whereas in *sae2*Δ mutants, bridging is disrupted but 5' resection is also low (Figures 3C-F), and neither single mutants show large deletions. By contrast, large deletions do form when both mutants are combined with the deletion of *NEJ1*. The end-bridging defect in *sae2*Δ mutants was epistatic with *nej1*Δ, yet the rate of 5' resection increased in *sae2*Δ *nej1*Δ compared to *sae2*Δ, and large deletions also formed. Consistent with this model, *mre11*-3 *nej1*Δ and *mre11*-3 *sae2*Δ had similar end-bridging defects, however both 5' resection and Dna2 levels remained low and large deletions did not develop in *mre11*-3 *sae2*Δ survivors. These data underscore the role of Sae2, together with Nej1, in end-bridging and also suggest an additional role for Sae2 in resection that goes beyond activation of Mre11 nuclease, as resection decreases more in *sae2*Δ compared to *mre11*-3 mutants.

We then determined whether the interplay between these factors also involved physical interactions by performing yeast-two-hybrid (Y2H) [4, 35]. Sae2 was overexpressed as HA-tagged prey and Nej1, the MRX subunits, and Dna2 domains - 1-450 aa (N-term), 451-900 aa (nuclease) and 901-1522 aa (helicase) were expressed as LexA-tagged bait [4], under control of a galactose-inducible promoter (Figure S3). Consistent with previous reports [36], Sae2 physically interacts with each component of MRX complex (Figure 3G). We also find Sae2 binds Nej1 more strongly than its binds the MRX components, and it physically interacts with the N-terminal regulatory region and nuclease domains of Dna2. Interestingly, Sae2-Dna2 and Sae2-MRX interactions increased in *nej1*Δ mutants (Figure 3G), which was similar to previous observations with Dna2-Sgs1 and Dna2-Mre11, which also increased when *NEJ1* was deleted [4]. Nej1 inhibits interactions between nucleases and nuclease regulators, however one difference to note is that Nej1 and Sae2 interact physically (Figure 3G), whereas Nej1 and Dna2 did not [4]. Taken together, these data support a model whereby Nej1 inhibits Dna2 recruitment to DSBs through multiple pathways. In addition to Nej1 inhibiting Sgs1-dependent Dna2 recruitment, Nej1 interacts with Mre11 and Sae2 inhibiting Dna2 binding with these factors (Figure 3H and [4]).

Dna2 plays a major role in resection at DSB that is inhibited by Nej1

We observed that recruitment of Dna2 at DSB is partially dependent on Sae2 and Sgs1, and both pathways are inhibited by Nej1. Furthermore, the rate of resection is severely hampered in cells harboring the *dna2*-1 mutation which is modestly alleviated by *NEJ1* deletion, indicating both Dna2 levels and nuclease function are critically important for processing events at a DSBs. Taken together we were prompted to determine whether *nej1*Δ, which removes Dna2 inhibition, would alleviate *sae2*Δ *sgs1*Δ synthetic lethality (SL) [27]. We crossed *sae2*Δ *nej1*Δ with *sgs1*Δ *nej1*Δ and spores with the triple mutant combination grew remarkably well (Figure 4A). Similar to *nej1*Δ and the *sae2*Δ *nej1*Δ with *sgs1*Δ *nej1*Δ double mutants, the triple mutant showed a low level of survival and an accumulation of large deletions under chronic HO induction (Figures 4B, C). The rate of resection in the triple mutant was indistinguishable from wild type and significantly higher than levels in *sae2*Δ and *sgs1*Δ single mutants (Figure 4D). Moreover, $Dna2^{HA}$ recruitment to a DSB in *sae2*Δ *sgs1*Δ *nej1*Δ mutants was similar to WT (Figure 4E), and above levels in *sae2*Δ +/- *NEJ1* or *sgs1*Δ (Figures 1C, 3B). To determine whether the reversion *sae2*Δ *sgs1*Δ lethality from *NEJ1* deletion was Dna2 nuclease dependent, we generated heterozygous diploids for *sae2*Δ, *sgs1*Δ, *nej1*Δ and *dna2-1* and upon tetrad dissection no viable spores with the quadruple mutant combination were recovered (Figure 4F). Taken together, our data support a model whereby Dna2 is recruited to a DSB through three pathways all under inhibition by Nej1. Dna2 localizes primarily through binding with Sae2 and Sgs1, thus deletion of both results in lethality. Removal of Nej1, which binds Mre11-C , allows Dna2 recruitment through Mre11-Dna2 interactions with cell viability in *sae2*Δ, *sgs1*Δ, *nej1*Δ mutants now dependent on the nuclease activity of Dna2 (Figure 4G).

DISCUSSION

Here we show Nej1 is a general inhibitor of 5' resection by regulating the recruitment of central nucleases and their binding partners to a DSB. We show that Dna2 is recruited to a DSB by Sae2, independently of Sgs1, and that Nej1 physically interacts with Sae2. Nej1 not only inhibits Dna2 interactions with Sgs1 and MRX [4], but the data presented here show Nej1 also inhibits MRX- Sae2 interaction and Sae2-dependent Dna2 recruitment. Moreover, deletion of *NEJ1* and

SAE2 show epistatic end-bridging defects, raising the possibility that their interaction might also have functional relevance for this important mechanism in DSB repair.

The relationship between Dna2 and NHEJ factors

The 5' resection defects in *dna2*-1 mutants support a Sgs1-independent role for Dna2 in DSB repair and indicate that only part of Dna2 functionality in resection is manifested by deletion of *SGS1*. Resection was more defective in *dna2*-1 compared to *sgs1*Δ even though Dna2 levels were similarly reduced in *dna2*-1 and *sgs1*Δ (Figures 1B, C). Moreover, Dna2 is still recruited to a DSB, *albeit* at lower levels, in the absence of Sgs1. Underscoring the inhibitory relationship between Nej1 and Dna2, when *NEJ1* was deleted in *sgs1*Δ mutants, Dna2 levels increased to above wild type indicating that Nej1 inhibits Dna2 recruitment through Sgs1-independent pathway(s) (Figure 1C and [4]).

Double mutant combination of either *dna2*-1 or *sgs1*Δ with *EXO1* deletion also support an Sgs1-independent function for Dna2 at the DSB. 5' resection was markedly reduced in both *exo1*Δ *dna2*-1 and *exo1*Δ *sgs1*Δ as the two long-range resection pathways were disrupted. However, deletion of *NEJ1* reversed the resection defect more in *exo1*Δ *sgs1*Δ *nej1*Δ triple mutants (Figures 2B). There appears to be little or no genetic interaction between *NEJ1* and *EXO1* in DSB repair as hyper-resection in *nej1*Δ mutants was not reversed by the deletion of *EXO1* and large deletions persisted (Figures 2B, D) [9]. Another difference to highlight is that *exo1*Δ *dna2*-1 survivors contained very few mutations at the break site whereas *exo1*Δ *sgs1*Δ survivors contained a high percentage of small indels indicative of some short-range resection, independently of *NEJ1* status (Figure 2C). Of note, *exo1*Δ *dna2*-1 double mutants were viable, which is in contrast to the lethal interaction previously reported for *exo1*Δ *dna2*Δ *pif1*-m2 [16]. How the *pif1*-m2 mutation might impact the genetic interaction between *DNA2* and *EXO1* is not clear, however this result suggests that the genetic lethality does not stem from loss of Dna2 nuclease activity.

Our data also suggests that Dna2 and Nej1 have an antagonistic relationship rather than a unidirectional one where Nej1 inhibits Dna2, as the levels of Nej1 and Ku70 increase at DSBs in *dna2*-1 (Figures S1B-C). These results suggest that increased levels of Ku and Nej1 and delayed

resection allow more opportunity for NHEJ. Indeed, survival of *dna2*-1 mutants increases under HO-DSB induction when NHEJ is proficient, as in *NEJ1*+ (Figures 1C). Canonical NHEJ factors down-regulate 5' resection at DSBs, however with the exception of Ku, mechanistic understanding about how these factors contribute to repair pathway choice remains fairly obscure. We show Nej1, which is known to contributes to Ku stability [3], has different genetic requirements for inhibiting resection compared to those previously identified for Ku. For example, even though *nej1*Δ, like *ku70*Δ, suppresses the sensitivity *mre11*-3 and *sae2*Δ, (Figure 2A, 3C and [37, 38]), the rescue of *mre11*-3 by *ku70*Δ depends on Exo1 nuclease, yet rescue by *nej1*Δ is Exo1-independent [9,37, 38].

Nej1 and Sae2 in end-bridging

Nej1 physically interacts with Sae2 and down regulates Sae2 interactions with MRX. Consistent with recent reports, Sae2 has a role in end-bridging (Figure 3F; [31-33]). In contrast to the additive end-bridging defects for *rad50*Δ *nej1*Δ [4], sae2Δ end-bridging defects are epistatic with *nej1*Δ. Given the physical interaction between Nej1 and Sae2, it is possible that the two factors could function as a complex in end bridging. It might be informative to determine whether Sae2 and Nej1 can form hetero-oligomers, distinguishing a sub-population of Sae2 involved in DNA end-bridging apart from Sae2 homo-oligomers involved in Mre11 activation and checkpoint signalling [39, 40]. Importantly, none of the other factors involved in 5' resection, when mutated, showed a defect in end-bridging including *exo1*Δ, *sgs1*Δ, *mre11*-3, or *dna2*-1 (Figure S2). These data are in line with previous work showing the structural integrity of the MRX complex, which remains intact in *mre11*-3, is important for its end-bridging function [12, 13, 41].

Sae2-dependent recruitment of Dna2 is inhibited by Nej1

As MRX is required for the recruitment of other processing factors to the DSB, *mre11*-3 was used in this study because in contrast to *mre11*Δ the complex is proficient in localizing and end-bridging in this nuclease-dead allele [12, 13, 41]. Consistent with previous reports, we find Dna2 recruitment to DNA ends did not depend on Mre11 nuclease activity, however levels were reduced in *sae2*Δ (Figure 3A; [42]). This differs slightly from previous work, which showed Dna2

is reduced at 2 hours, but not at 3 hrs, in *sae2*Δ mutant cells [42]. This discrepancy could result from slight variations in the experimental set up because in the same study Ku70 was not altered 3 hrs after HO induction in *sae2*Δ mutants, yet we find that Ku70 levels increase slightly (Figure S1C). Our results are however in line with work showing *KU70* deletion suppresses the damage sensitivity of *sae2*Δ and Ku70 levels increase at a DSB in *ctp1*Δ mutants in S. *pombe* [37, 38, 43].

Recent *in-vitro* studies have shown that human CtIP has a stimulatory effect on Dna2 nuclease [29, 30]. We observed a physical interaction between Sae2 and Dna2 which was inhibited by Nej1 (Figure 3G). Dna2 enrichment levels at a DSB corresponded well with resection levels in the various mutant backgrounds (Figures 3B, C), and support a model for Sae2 recruitment of Dna2 to DSBs. Indeed, there was a marked decrease in Dna2 in *sae2*Δ mutant cells compared to *mre11*-3 (Figures 2E, 3B). These data are consistent with previous work showing Dna2 recruitment to DSBs occurs through interactions with CtIP in humans [44]. Nej1 inhibited Dna2 recruitment in the various mutant backgrounds. Compared to *sae2*Δ mutants, the level of Dna2 increased in *sae2*Δ *nej1*Δ, however recovery levels remained lower than in *mre11*-3 *nej1*Δ (Figures 2E, 3B). Our data do not contradict the role of Sae2 as a nuclease [28], but further study of the interplay between Nej1, Dna2 and Sae2-mutants (D285P/K288P and E161P/K163P) is imperative.

Dna2 recovery and 5' resection in *sae2*Δ *sgs1*Δ *nej1*Δ was restored to wild type levels, which was quite surprising given *sae2*Δ *sgs1*Δ is synthetic lethal (Figure 4) [27]. It is puzzling that the recovery of Dna2 and the rate of resection is greater in *sae2*Δ sgs1Δ *nej1*Δ compared to *sae2*Δ *nej1*Δ. These data might indicate that the presence of Sgs1 is inhibitory to the initiation of resection when *SAE2* has been deleted. We previously showed that both Sgs1 and Dna2 interact directly with Mre11 [4]. Thus, one possibility is that the relative amount of Dna2 binding directly to Mre11 is dynamic and altered in *sae2*Δ *nej1*Δ mutants and impacted differently by the presence of Sgs1. For example, Dna2-Mre11 might function to initiate resection in *sae2*Δ, whereas Dna2 in complex with Sgs1 at the DSB functions in long-range resection and is less efficient in initiating it. In the absence of Mre11 nuclease activity however, Sgs1-Dna2 would become very important for resection, and as previously shown, this

interaction is also inhibited by Nej1 [4, 9]. Consistent with such a model, both Dna2 and 5' resection levels increase in *mre11*-3 *sae2*Δ *nej1*Δ, relative to *mre11*-3 *sae2*Δ.

Suppression of *sae2*Δ *sgs1*Δ lethality, has also been seen upon deletion of other factors that inhibit resection, *KU70* and *RAD9*. Like triple mutant combinations with *ku70*Δ or *rad9*Δ, resection in *sae2*Δ *sgs1*Δ *nej1*Δ was similar to wild type at later time points. The increased resection and rescue of *sae2*Δ *sgs1*Δ upon *NEJ1* deletion might result from decreased end-joining, as this would also be reduced in *ku70*Δ. However, two results suggest that the loss of end-joining itself does not rescue the lethality of *sae2*Δ *sgs1*Δ. First, deletion of *DNL4* ligase does not rescue *sae2*Δ *sgs1*Δ and in *sae2*Δ *sgs1*Δ *rad9*Δ triple mutants, NHEJ occurs.

We show Dna2 can be recruited to the DSB site by Sae2, and like its recruit through Mre11 and Sgs1, Dna2-Sae2 is inhibited by Nej1. We also report well-regulated and balanced interplay between Nej1, Sae2 and Dna2 in end-bridging and end-resection. This work underlines a central function for Dna2 nuclease in DSB repair and accentuates the role Nej1 as a major regulator of NHEJ/repair pathway choice.

MATERIALS AND METHODS

KEY RESOURCE TABLE

REAGENT or RESOURCE	SOURCE	IDENTIFIER
Antibodies		
HA-probe mouse monoclonal antibody	Santa Cruz Biotechnology	F-7
LexA-Probe mouse monoclonal antibody	Santa Cruz Biotechnology	2-12
Myc-Probe mouse monoclonal antibody	Abcam	ab32
Peroxidase conjugated AffiniPure Goat anti-Mouse antibody	Jackson ImmunoResearch	115035174
Chemicals		
Adenine	Sigma	A8626
Bacto™ Peptone	BD Biosciences	211677
Bacto™ Yeast extract	BD Biosciences	212750
Complete EDTA free protease inhibitor cocktail	Roche	04693159001
Dextrose	Sigma	D1912
Difco™ Agar	BD Biosciences	214530
Dynabeads Sheep anti-Mouse IgG	Invitrogen	20230531
EDTA	VWR	0322
Ethanol	Commercial alcohols	P006EAAN
Formaldehyde	Sigma	F8775
Galactose	Sigma	G0750
Glycine	VWR	CA93291
Glycogen	Roche	10901393001
Lactic acid	Sigma	69785
Lithium Chloride	EMD Millipore	LX03311
Phenol-Chloroform-Isoamylalcohol	Invitrogen	15593049
PMSF	Sigma	78830
Potassium Chloride	EMD Chemicals	1049360500
Raffinose	US Biological	R1030
SDS	Avantor	409502
Sodium Acetate	VWR	BDH9278
Sodium Chloride	Fisher Chemical	S64212
Tris base	Fisher Chemical	BP1525
Triton	Sigma	9002931
Zirconia Silica beads	BioSpec Products	11079105z
Enzymes		
Proteinase K	Invitrogen	25530031
RNase A	Sigma	R6513
RsaI	New England Biolabs	R0167S
Kits		
PerfeCTa qPCR SuperMix, ROX	Quanta BioSciences Inc.	89168-786
PowerUp SYBR Green Master Mix	Applied Biosystems	A25743
Western Lightning Plus-ECL	PerkinElmer	NEL105001EA

Plasmids		
Plasmids used in this study	Table S2	
Primers		
Primers used in this study	Table S3	
Yeast strains		
Yeast strains used in this study	Table S1	

All the yeast strains used in this study are listed in Table S1 and were obtained by crosses. The strains were grown on various media in experiments described below. For HO-induction of a DSB, YPLG media is used (1% yeast extract, 2% bactopeptone, 2% lactic acid, 3% glycerol and 0.05% glucose). For the continuous DSB assay, YPA plates are used (1% yeast extract, 2% bacto peptone, 0.0025% adenine) supplemented with either 2% glucose or 2% galactose. For the mating type assays, YPAD plates are used (1% yeast extract, 2% bacto peptone, 0.0025% adenine, 2% dextrose). For yeast 2-hybrid assays, standard amino acid drop-out media lacking histidine, tryptophan and uracil is used and 2% raffinose is added as the carbon source for the cells.

METHOD DETAILS

Chromatin Immunoprecipitation

ChIP assay was performed as described previously [4]. Cells were cultured overnight in YPLG at 25°C. Cells were then diluted to equal levels (5 x 10^6 cells/ml) and were cultured to one doubling (3-4 hrs) at 30°C. 2% GAL was added to the YPLG and cells were harvested and crosslinked at various time points using 3.7% formaldehyde solution. Following crosslinking, the cells were washed with ice cold PBS and the pellet stored at -80°C. The pellet was re-suspended in lysis buffer (50mM Hepes pH 7.5, 1mM EDTA, 80mM NaCl, 1% Triton, 1mM PMSF and protease inhibitor cocktail) and cells were lysed using Zirconia beads and a bead beater. Chromatin fractionation was performed to enhance the chromatin bound nuclear fraction by spinning the cell lysate at 13,200rpm for 15 minutes and discarding the supernatant. The pellet was re-suspended in lysis buffer and sonicated to yield DNA fragments (~500bps in length). The sonicated lysate was then incubated in beads + anti-HA/Myc Antibody or unconjugated beads (control) for 2 hrs at 4°C. The beads were washed using wash buffer (100mM Tris pH 8, 250mM LiCl, 150mM (HA Ab) or 500mM (Myc Ab) NaCl, 0.5% NP-40, 1mM EDTA, 1mM PMSF and protease inhibitor cocktail) and protein-DNA complex was eluted by reverse crosslinking using 1%SDS in TE buffer, followed by proteinase K treatment and DNA isolation via phenol-chloroform-isoamyl alcohol extraction. Quantitative PCR was performed using the Applied Biosystem QuantStudio 6 Flex machine. PerfeCTa qPCR SuperMix, ROX was used to visualize enrichment at HO2 (0.5kb from DSB) and HO1 (1.6kb from DSB) and SMC2 was used as an internal control.

Tethering Microscopy

Cells derived from the parent strain JC-4066 were diluted and grown overnight in YPLG at 25°C to reach a concentration of $1x10^7$ cells/ml. Cells were treated with 2% GAL for 2 hours and cell pellets were collected and washed 2 times with PBS. After the final wash, cells were placed on cover slips and imaged using a fully motorized Nikon Ti Eclipse inverted epi-fluorescence microscope. Z-stack images were acquired with 200 nm increments along the z plane, using a 60X oil immersion 1.4 N.A. objective. Images were captured with a Hamamatsu Orca flash 4.0 v2 sCMOS 16-bit camera and the system was controlled by Nikon NIS-Element Imaging Software (Version 5.00). All images were deconvolved with Huygens Essential version 18.10 (Scientific Volume Imaging, The Netherlands, http://svi.nl), using the Classic Maximum Likelihood Estimation (CMLE) algorithm, with SNR:40 and 50 iterations. To measure the distance between the GFP and mCherry foci, the ImageJ plug-in Distance Analysis (DiAna) was used [45]. Distance measurements represent the shortest distance between the brightest pixel in the mCherry channel and the GFP channel. Each cell was measured individually and > 50 cells were analyzed per condition per biological replicate.

qPCR based Resection Assay

Cells from each strain were grown overnight in 15ml YPLG to reach an exponentially growing culture of $1x10^7$ cells/mL. Next, 2.5mL of the cells were pelleted as timepoint 0 sample, and 2% GAL was added to the remaining cells, to induce a DSB. Following that, respective timepoint samples were collected. Genomic DNA was purified using standard genomic preparation method by isopropanol precipitation and ethanol washing, and DNA was re-suspended in 100mL ddH_2O. Genomic DNA was treated with 0.005µg/µL RNase A for 45min at 37°C. 2µL of DNA was added to tubes containing CutSmart buffer with or without RsaI restriction enzyme and incubated at 37°C for 2hrs. Quantitative PCR was performed using the Applied Biosystem QuantStudio 6 Flex machine. PowerUp SYBR Green Master Mix was used to quantify resection at MAT1 (0.15kb from DSB) locus. Pre1 was used as a negative control. RsaI cut DNA was normalized to uncut DNA as previously described to quantify the %ssDNA / total DNA [31].

Continuous DSB assay and identification of mutations in survivors

Cells were grown overnight in YPLG media at 25°C to saturation. Cells were collected by centrifugation at 2500rpm for 3 minutes and pellets were washed 1x in ddH_2O and re-suspended in ddH_2O. Cells were counted and spread on YPA plates supplemented with either 2% GLU or 2% GAL. On the Glucose plates $1x10^3$ total cells were added and on the galactose plates $1x10^5$ total cells were added. The cells were incubated for 3-4 days at room temperature and colonies counted on each plate. Survival was determined by normalizing the number of surviving colonies in the GAL plates to number of colonies in the GLU plates. 100 survivors from each strain were scored for the mating type assay as previously described [9].

Yeast 2-hybrid

Various plasmids (Table S2) were constructed containing the gene encoding the region of the proteins – Sae2, Dna2, Mre11, Nej1, Rad50 and Xrs2, using the primers listed in Table S3. The plasmids J-965 and J-1493 and the inserts were treated with BamHI and EcoRI and ligated using

T4 DNA ligase. The plasmids were sequence verified. Reporter (J-359), bait (J-965) and prey (J-1493) plasmids, containing the gene encoding the desired protein under a galactose inducible promoter, were transformed into JC-1280. Cells were grown overnight in –URA –HIS –TRP media with 2% raffinose. Next day, cells were transferred into –URA –HIS –TRP media with either 2% GLU or 2% GAL and grown for 6 hrs at 30°C. Cell pellets were resuspended and then permeabilized using 0.1% SDS followed by ONPG addition. β-galactosidase activity was estimated by measuring the OD at 420nm, relative β-galactosidase units were determined by normalizing to total cell density at OD600. Additionally, for drop assay cells were grown and spotted in five-fold serial dilutions on plates containing 2% galactose lacking histidine and tryptophan (for plasmid selection) and leucine (for measuring expression from *lexAop6-LEU2*). Plates were photographed after 3-4 days of incubation at 30°C.

Western Blot

Cells were lysed by re-suspending them in lysis buffer (with PMSF and protease inhibitor cocktail tablets) followed by bead beating. The protein concentration of the whole cell extract was determined using the NanoDrop. Equal amounts of whole cell extract were added to wells of 10% polyacrylamide SDS gel. After the run, the protein were transferred to Nitrocellulose membrane at 100V for 80mins. The membrane was Ponceau stained (which served as a loading control), followed by blocking in 10% milk-PBST for 1hour at room temperature. Respective primary antibody solution (1:1000 dilution) was added and left for overnight incubation at 4°C. The membranes were then washed with PBST and left for 1 hour with secondary antibody. Followed by washing the membranes, adding the ECL substrates and imaging them.

AUTHORS CONTRIBUTIONS

A.M. and J.A.C. designed the research. A.M., and N.A. performed experiments and analyzed the data. A.M., N.A. and J.A.C wrote the manuscript.

ACKNOWLEDGEMENTS

This work was supported by operating grants from CIHR MOP-82736; MOP-137062 and NSERC 418122 awarded to J.A.C. The authors declare that they have no conflicts of interest with the contents of this article. We acknowledge the resources provided by the Live Cell Imaging Laboratory. The Nikon Ti Eclipse inverted epi-fluorescence microscope system was purchased with funds from the International Microbiome Centre, which is supported by the Cumming School of Medicine at University of Calgary, Western Economic Diversification (WED) and Alberta Economic Development and Trade (AEDT), Canada.

REFERENCES

1. Wu D, Topper LM, Wilson TE. Recruitment and dissociation of nonhomologous end joining proteins at a DNA double-strand break in Saccharomyces cerevisiae. Genetics. 2008; 178(3): 1237-1249. doi: 10.1534/genetics.107.083535.
2. Palmbos, PL., Wu, D., Daley, JM., Wilson, TE. (2008) Recruitment of Saccharomyces cerevisiae Dnl4-Lif1 complex to a double-strand break requires interactions with Yku80 and the Xrs2 FHA domain. Genetics. 2008; 180: 1809–1819.
3. Chen, X., Tomkinson, AE. Yeast Nej1 is a key participant in the initial end binding and final ligation steps of nonhomologous end joining. J. Biol. Chem. 2011; 286: 4931–4940.
4. Mojumdar A., Sorenson K., Hohl M., Toulouze M., Lees-Miller SP., Dubrana K., Petrini JHJ., Cobb JA. Nej1 Interacts with Mre11 to Regulate Tethering and Dna2 Binding at DNA Double-Strand Breaks. Cell Rep. 2019 Aug 6; 28(6): 1564-1573.e3. doi: 10.1016/j.celrep.2019.07.018.
5. Frank-Vaillant M, Marcand S. NHEJ regulation by mating type is exercised through a novel protein, Lif2p, essential to the ligase IV pathway. Genes Dev. 2001; 15(22): 3005-3012. doi: 10.1101/gad.206801.
6. Valencia M, Bentele M, Vaze MB, Herrmann G, Kraus E, Lee SE, Schär P, Haber JE. NEJ1 controls non-homologous end joining in Saccharomyces cerevisiae. Nature. 2001; 414(6864): 666-669. doi: 10.1038/414666a.
7. Zhang Y, Hefferin ML, Chen L, Shim EY, Tseng HM, Kwon Y, Sung P, Lee SE, Tomkinson AE. Role of Dnl4-Lif1 in nonhomologous end-joining repair complex assembly and suppression of homologous recombination. Nat Struct Mol Biol. 2007; 14(7): 639-646. doi: 10.1038/nsmb1261.
8. Mahaney BL, Lees-Miller SP, Cobb JA. The C-terminus of Nej1 is critical for nuclear localization and non-homologous end-joining. DNA Repair (Amst). 2014; 14: 9-16. doi: 10.1016/j.dnarep.2013.12.002.
9. Sorenson KS, Mahaney BL, Lees-Miller SP, Cobb JA. The non-homologous end-joining factor Nej1 inhibits resection mediated by Dna2-Sgs1 nuclease-helicase at DNA double strand breaks. J Biol Chem. 2017; 292(35): 14576-14586.
10. Hopfner KP, Karcher A, Craig L, Woo TT, Carney JP, Tainer JA. Structural biochemistry and interaction architecture of the DNA double-strand break repair Mre11 nuclease and Rad50-ATPase. Cell. 2001; 105: 473–485.
11. Wiltzius JJ, Hohl M, Fleming JC, Petrini JH. The Rad50 hook domain is a critical determinant of Mre11 complex functions. Nat Struct Mol Biol. 2005; 12(5): 403-407. doi: 10.1038/nsmb928.
12. Hohl M, Kwon Y, Galván SM, Xue X, Tous C, Aguilera A, Sung P, Petrini JH. The Rad50 coiled-coil domain is indispensable for Mre11 complex functions. Nat. Struct. Mol. Biol. 2011; 18: 1124–1131.
13. Hohl M, Kochańczyk T, Tous C, Aguilera A, Krężel A, Petrini JH. Interdependence of the rad50 hook and globular domain functions. Mol. Cell. 2015; 57: 479–491.

14. Cannavo E, Cejka P. Sae2 promotes dsDNA endonuclease activity within Mre11-Rad50-Xrs2 to resect DNA breaks. Nature. 2014; 514: 122–125.
15. Cejka P. DNA End Resection: Nucleases Team Up with the Right Partners to Initiate Homologous Recombination. J Biol Chem. 2015; 290(38): 22931-22938. doi: 10.1074/jbc.R115.675942.
16. Zhu Z, Chung WH, Shim EY, Lee SE, Ira G. Sgs1 helicase and two nucleases Dna2 and Exo1 resect DNA double-strand break ends. Cell. 2008; 134: 981–994.
17. Budd ME, Campbell JL. A new yeast gene required for DNA replication encodes a protein with homology to DNA helicases. Proc Natl Acad Sci U S A. 1995; 92(17): 7642-7646. doi:10.1073/pnas.92.17.7642.
18. Budd ME, Choe WC, Campbell JL. The nuclease activity of the yeast DNA2 protein, which is related to the RecB-like nucleases, is essential in vivo. J Biol Chem. 2000; 275(22): 16518-16529. doi: 10.1074/jbc.M909511199.
19. Jia PP, Junaid M, Ma YB, Ahmad F, Jia YF, Li WG, Pei DS. Role of human DNA2 (hDNA2) as a potential target for cancer and other diseases: A systematic review. DNA Repair (Amst). 2017; 59: 9-19. doi: 10.1016/j.dnarep.2017.09.001.
20. Kumar S, Peng X, Daley J, Yang L, Shen J, Nguyen N, Bae G, Niu H, Peng Y, Hsieh HJ, et al. Inhibition of DNA2 nuclease as a therapeutic strategy targeting replication stress in cancer cells. Oncogenesis. 2017; 6: e319. https://doi.org/10.1038/oncsis.2017.15.
21. Bae SH, Bae KH, Kim JA, Seo YS. RPA governs endonuclease switching during processing of Okazaki fragments in eukaryotes. Nature. 2001; 412(6845): 456-61. doi: 10.1038/35086609.
22. Budd ME, Reis CC, Smith S, Myung K, Campbell JL. Evidence suggesting that Pif1 helicase functions in DNA replication with the Dna2 helicase/nuclease and DNA polymerase delta. Mol Cell Biol. 2006; 26(7): 2490-500. doi: 10.1128/MCB.26.7.2490-2500.2006.
23. Bae SH, Choi E, Lee KH, Park JS, Lee SH, Seo YS. Dna2 of Saccharomyces cerevisiae possesses a single-stranded DNA-specific endonuclease activity that is able to act on double-stranded DNA in the presence of ATP. J Biol Chem. 1998; 273(41): 26880-90. doi: 10.1074/jbc.273.41.26880.
24. Budd ME, Campbell JL. Interplay of Mre11 nuclease with Dna2 plus Sgs1 in Rad51-dependent recombinational repair. PLoS One. 2009; 4(1): e4267. doi: 10.1371/journal.pone.0004267.
25. Budd ME, Campbell JL. The pattern of sensitivity of yeast dna2 mutants to DNA damaging agents suggests a role in DSB and postreplication repair pathways. Mutat Res. 2000; 459(3): 173-86. doi: 10.1016/s0921-8777(99)00072-5.
26. Gobbini E, Villa M, Gnugnoli M, Menin L, Clerici M, Longhese MP. Sae2 Function at DNA Double-Strand Breaks Is Bypassed by Dampening Tel1 or Rad53 Activity. PLoS Genet. 2015; 11(11): e1005685. https://doi.org/10.1371/journal.pgen.1005685.
27. Yu TY, Kimble MT, Symington LS. Sae2 antagonizes Rad9 accumulation at DNA double-strand breaks to attenuate checkpoint signaling and facilitate end resection. Proc Natl Acad Sci U S A. 2018; 115(51): E11961-E11969. doi: 10.1073/pnas.1816539115.

28. Arora S, Deshpande RA, Budd M, Campbell J, Revere A, Zhang X, Schmidt KH, Paull TT. Genetic Separation of Sae2 Nuclease Activity from Mre11 Nuclease Functions in Budding Yeast. Mol Cell Biol. 2017; 37(24): e00156-17. doi: 10.1128/MCB.00156-17.
29. Daley JM, Jimenez-Sainz J, Wang W, Miller AS, Xue X, Nguyen KA, Jensen RB, Sung P. Enhancement of BLM-DNA2-Mediated Long-Range DNA End Resection by CtIP. Cell Rep. 2017; 21(2): 324-332. doi: 10.1016/j.celrep.2017.09.048.
30. Ceppi I, Howard SM, Kasaciunaite K, Pinto C, Anand R, Seidel R, Cejka P. CtIP promotes the motor activity of DNA2 to accelerate long-range DNA end resection. Proc Natl Acad Sci U S A. 2020; 117(16): 8859-8869. doi: 10.1073/pnas.2001165117.
31. Ferrari M, Dibitetto D, De Gregorio G, Eapen VV, Rawal CC, Lazzaro F, Tsabar M, Marini F, Haber JE, Pellicioli A. Functional interplay between the 53BP1-ortholog Rad9 and the Mre11 complex regulates resection, end-tethering and repair of a double-strand break. PLoS Genet. 2015; 11(1): e1004928. doi: 10.1371/journal.pgen.1004928.
32. Öz R, Howard SM, Sharma R, Törnkvist H, Ceppi I, Kk S, Kristiansson E, Cejka P, Westerlund F. Phosphorylated CtIP bridges DNA to promote annealing of broken ends. Proc Natl Acad Sci U S A. 2020; 117(35): 21403-21412. doi: 10.1073/pnas.2008645117.
33. Andres SN, Li ZM, Erie DA, Williams RS. Ctp1 protein-DNA filaments promote DNA bridging and DNA double-strand break repair. J Biol Chem. 2019; 294(9): 3312-3320. doi: 10.1074/jbc.RA118.006759.
34. Moore JK, Haber JE. Cell cycle and genetic requirements of two pathways of nonhomologous end-joining repair of double-strand breaks in Saccharomyces cerevisiae. Mol. Cell. Biol. 1996; 16: 2164–2173.
35. Bustard D, Menolfi D, Jeppsson K, Ball LG, Dewey SC, Shirahige K, Sjogren C, Branzei D, Cobb JA. During replication stress Non-Smc-Element 5 is required for Smc5/6 complex functionality at stalled forks. J Biol Chem. 2012; 287: 11374-11383.
36. Cannavo E, Johnson D, Andres SN, Kissling VM, Reinert JK, Garcia V, Erie DA, Hess D, Thomä NH, Enchev RI, et al. Regulatory control of DNA end resection by Sae2 phosphorylation. Nat Commun. 2018; 9(1): 4016. doi: 10.1038/s41467-018-06417-5.
37. Mimitou EP, Symington LS. Ku prevents Exo1 and Sgs1-dependent resection of DNA ends in the absence of a functional MRX complex or Sae2. EMBO J. 2010; 29(19): 3358-69.
38. Foster SS, Balestrini A, Petrini JH. Functional interplay of the Mre11 nuclease and Ku in the response to replication-associated DNA damage. Mol Cell Biol. 2011; 31(21): 4379-89. doi: 10.1128/MCB.05854-11.
39. Kim HS, Vijayakumar S, Reger M, Harrison JC, Haber JE, Weil C, Petrini JH. Functional interactions between Sae2 and the Mre11 complex. Genetics. 2008; 178(2): 711-723. doi: 10.1534/genetics.107.081331.
40. Fu Q, Chow J, Bernstein KA, Makharashvili N, Arora S, Lee CF, Person MD, Rothstein R, Paull TT. Phosphorylation-regulated transitions in an oligomeric state control the activity of the Sae2 DNA repair enzyme. Mol Cell Biol. 2014; 34(5): 778-793. doi: 10.1128/MCB.00963-13.

41. Lobachev K, Vitriol E, Stemple J, Resnick MA, Bloom K. Chromosome fragmentation after induction of a double-strand break is an active process prevented by the RMX repair *complex. Curr Biol. 2004*; 14(23): 2107-12.
42. Shim EY, Chung WH, Nicolette ML, Zhang Y, Davis M, Zhu Z, Paull TT, Ira G, Lee SE. Saccharomyces cerevisiae Mre11/Rad50/Xrs2 and Ku proteins regulate association of Exo1 and Dna2 with DNA breaks. EMBO J. 2010; 29(19): 3370-3380. doi: 10.1038/emboj.2010.219.
43. Langerak P, Mejia-Ramirez E, Limbo O, Russell P. Release of Ku and MRN from DNA ends by Mre11 nuclease activity and Ctp1 is required for homologous recombination repair of double-strand breaks. PLoS Genet. 2011; 7(9): e1002271. doi: 10.1371/journal.pgen.1002271.
44. Hoa NN, Kobayashi J, Omura M, Hirakawa M, Yang SH, Komatsu K, Paull TT, Takeda S, Sasanuma H. BRCA1 and CtIP Are Both Required to Recruit Dna2 at Double-Strand Breaks in Homologous Recombination. PLoS One. 2015; 10(4): e0124495. doi: 10.1371/journal.pone.0124495.
45. Gilles JF, Dos Santos M, Boudier T, Bolte S, Heck N. DiAna, an ImageJ tool for object-based 3D co-localization and distance analysis. Methods. 2017; 115: 55-64. doi: 10.1016/j.ymeth.2016.11.016.

FIGURE LEGENDS

Figure 1. Sgs1-independent recruitment of Dna2 nuclease is inhibited by Nej1 at DSB.

(A) Schematic representation of regions around the HO cut site on chromosome III. **i**) Schematic representation of mating type analysis of survivors from persistent DSB induction assays. The mating phenotype is a read out for the type of repair: α survivors (mutated HO endonuclease-site, grey), sterile survivors (small insertions and deletions, blue) and "a-like" survivors (>700 bps deletion, red). **ii**) The ChIP probe used in this study is 0.6kb from the DSB. The RsaI sites used in the qPCR resection assays, 0.15kb from the DSB, are also indicated. Both sides of HO cut site are tagged with GFP (5kb from cute site) and mCherry (9kb from cut site) repeats, which were used in end-tethering microscopy.

(B) qPCR-based resection assay of DNA 0.15kb away from the HO DSB, as measured by % ssDNA, at 0, 40, 80 and 150 min post DSB induction in cycling cells in wild type (JC-727), *nej1*Δ (JC-1342), *sgs1*Δ (JC-3757), *sgs1*Δ *nej1*Δ (JC-3759), *dna2*-1 (JC-5655), *dna2*-1 *nej1*Δ (JC-5670), *dna2*-1 *sgs1*Δ (JC-5745) and *dna2*-1 *sgs1*Δ *nej1*Δ (JC-5746).

(C) Enrichment of $Dna2^{HA}$ at 0.6kb from DSB 0 hour (no DSB induction) and 3 hours after DSB induction in wild type (JC-4117), *nej1*Δ (JC-4118), *sgs1*Δ (JC-5624), *dna2*-1 (JC-5707), *sgs1*Δ *nej1*Δ (JC-5627) and no tag control (JC-727) was determined. The fold enrichment is normalized to recovery at the SMC2 locus.

(D) Percentage cell survival upon chronic HO induction in cells mentioned in (B).

(E) Mating type analysis of survivors from persistent DSB induction assays mentioned in (D and described in A).

For all the experiments - error bars represent the standard error of three replicates. Significance was determined using 1-tailed, unpaired Student's t test. All strains compared are marked (P<0.05*; P<0.01**; P<0.001***) and are compared to WT, unless specified with a line.

Figure 2. Dna2 recruitment to DSB is independent of Exo1.

(A) qPCR-based resection assay of DNA 0.15kb away from the HO DSB, as measured by % ssDNA, at 0, 40, 80 and 150 min post DSB induction in cycling cells in wild type (JC-727), *nej1*Δ (JC-1342), *mre11*-3 (JC-5372), *mre11*-3 *nej1*Δ (JC-5369), *mre11*-3 *sgs1*Δ (JC-5405), *mre11*-3 *sgs1*Δ *nej1*Δ (JC-5667), *mre11*-3 *dna2*-1 (JC-5748) and *mre11*-3 *dna2*-1 *nej1*Δ (JC-5532).

(B) qPCR based resection assay of DNA 0.15kb away from the HO DSB, as measured by % ssDNA, at 0, 40, 80 and 150 min post DSB induction in cycling cells in wild type (JC-727), *nej1*Δ (JC-1342), *exo1*Δ (JC-3767), *exo1*Δ *nej1*Δ (JC-5373), *exo1*Δ *sgs1*Δ (JC-4520), *exo1*Δ *sgs1*Δ *nej1*Δ (JC-5493), *exo1*Δ *dna2*-1 (JC-5692) and *exo1*Δ *dna2*-1 *nej1*Δ (JC-5630).

(C) Mating type analysis of survivors from persistent DSB induction assays mentioned in (D and described in 1A).

(D) Percentage cell survival upon chronic HO induction in cells mentioned in (A and B).

(E) Enrichment of Dna2^{HA} at 0.6kb from DSB 0 hour (no DSB induction) and 3 hours after DSB induction in wild type (JC-4117), *nej1*Δ (JC-4118), *mre11*-3 (JC-5594), *mre11*-3 *nej1*Δ (JC-5596), *mre11*-3 *sgs1*Δ (JC-5621), *mre11*-3 *sgs1*Δ *nej1*Δ (JC-5623), *exo1*Δ (JC-5626), *exo1*Δ *nej1*Δ (JC-5666), *exo1*Δ *sgs1*Δ (JC-5559), *exo1*Δ *sgs1*Δ *nej1*Δ (JC-5566) and no tag control (JC-727) was determined. The fold enrichment is normalized to recovery at the SMC2 locus.

For all the experiments - error bars represent the standard error of three replicates. Significance was determined using 1-tailed, unpaired Student's t test. All strains compared are marked (P<0.05*; P<0.01**; P<0.001***) and are compared to WT, unless specified with a line.

Figure 3. Sae2-dependent recruitment of Dna2 is inhibited by Nej1.

(A) Enrichment of Sae2^{HA} at 0.6kb from DSB 0 hour (no DSB induction) and 3 hours after DSB induction in wild type (JC-5116), *mre11*Δ (JC-5122), *mre11*-3 (JC-5119), *nej1*Δ (JC-5124), *mre11*-3 *nej1*Δ (JC-5702) and no tag control (JC-727). The fold enrichment represents normalization over the SMC2 locus.

(B) Enrichment of Dna2^{HA} at 0.6kb from DSB 0 hour (no DSB induction) and 3 hours after DSB induction in wild type (JC-4117), *nej1*Δ (JC-4118), *sae2*Δ (JC-5562), *sae2*Δ *nej1*Δ (JC-5597), *sae2*Δ *mre11*-3 (JC-5598), *sae2*Δ *mre11*-3 *nej1*Δ (JC-5593) and no tag control (JC-727) was determined. The fold enrichment is normalized to recovery at the SMC2 locus.

(C) qPCR-based resection assay of DNA 0.15kb away from the HO DSB, as measured by % ssDNA, at 0, 40, 80 and 150 min post DSB induction in cycling cells in wild type (JC-727), *nej1*Δ (JC-1342), *sae2*Δ (JC-5673), *sae2*Δ *nej1*Δ (JC-5675), *sae2*Δ *mre11*-3 (JC-5501), *sae2*Δ *mre11*-3 *nej1*Δ (JC-5500), *sae2*Δ *dna2*-1 (JC-5669) and *sae2*Δ *dna2*-1 *nej1*Δ (JC-5671).

(D) Percentage cell survival upon chronic HO induction in cells mentioned in (C).

(E) Mating type analysis of survivors from persistent DSB induction assays mentioned in (D and described in 1A).

(F) Representative image of yeast cells with tethered (co-localized GFP and mCherry) and untethered (distant GFP and mCherry) ends. Scatter plot showing the tethering of DSB ends, at 0 and 2 hours, as measured by the distance between the GFP and mCherry foci in wild type (JC-4066), *nej1*Δ (JC-4364), *sae2*Δ (JC-5524), *sae2*Δ *nej1*Δ (JC-5525), *mre11*-3 (JC-5529), *mre11*-3 *nej1*Δ (JC-5526), *sae2*Δ *mre11*-3 (JC-5530) and *sae2*Δ *mre11*-3 *nej1*Δ (JC-5531). The Geometric mean (GM) distance for each sample is specified under the respective sample data plot. Significance was determined using Kruskal-Wallis and Dunn's multiple comparison test.

(G) Y2H analysis of Sae2 fused to HA-AD and Mre11, Rad50, Xrs2, Nej1 and domains of Dna2, (Dna2-N terminal, Dna2-Nuclease and Dna2-Helicase domains) fused to lexA-DBD was performed in wild type cells (JC-1280) and in isogenic cells with *nej1*Δ (JC-4556) using a quantitative β-galactosidase assay and a drop assay on drop-out (-His, -Trp, -Leu) selective media plates.

(E) Model of DSB where Nej1 inhibits the physical association of Dna2-Sae2 and prevents Sae2-dependent Dna2 recruitment.

For all the experiments - error bars represent the standard error of three replicates. Significance was determined using 1-tailed, unpaired Student's t test. All strains compared are marked (P<0.05*; P<0.01**; P<0.001***) and are compared to WT, unless specified with a line.

Figure 4. Dna2 plays a major role in resection at DSB that is inhibited by Nej1.

(A) Viability and genotypes of spores derived from diploids of *sae2*Δ *nej1*Δ (JC-5675) and *sgs1*Δ *nej1*Δ (JC-3885).

(B) Percentage cell survival upon chronic HO induction in cells in wild type (JC-727), *nej1*Δ (JC-1342), *sae2*Δ (JC-5673), *sae2*Δ *nej1*Δ (JC-5675), *sgs1*Δ (JC-3757), *sgs1*Δ *nej1*Δ (JC-3759) and *sae2*Δ *sgs1*Δ *nej1*Δ (JC-5750).

(C) Mating type analysis of survivors from persistent DSB induction assays mentioned in (B and described in 1A).

(D) qPCR-based resection assay of DNA 0.15kb away from the HO DSB, as measured by % ssDNA, at 0, 40, 80 and 150 mins. post DSB induction in cycling cells mentioned in (B).

(E) Enrichment of $Dna2^{HA}$ at 0.6kb from DSB 0 hour (no DSB induction) and 3 hours after DSB induction in wild type (JC-4117), *sae2*Δ *sgs1*Δ *nej1*Δ (JC-5480) and no tag control (JC-727) was determined. The fold enrichment is normalized to recovery at the SMC2 locus.

(F) Viability and genotypes of spores derived from diploids of *sae2*Δ *sgs1*Δ *nej1*Δ (JC-5749) and *dna2*-1 (JC-5655).

(G) Model of DSB where Nej1 inhibits the physical association of Dna2-Mre11 and prevents Mre11-dependent Dna2 recruitment.

For all the experiments - error bars represent the standard error of three replicates. Significance was determined using 1-tailed, unpaired Student's t test. All strains compared are marked (P<0.05*; P<0.01**; P<0.001***) unless specified with a line, strains are compared to WT.

Supplementary Figure S1.

(A) Enrichment of Sgs1^{HA} at DSB, at 0 and 3 hours, in wild type (JC-4135), *dna2*-1 (JC-5681) and no tag control (JC-727).

(B) Enrichment of Nej1^{Myc} at DSB, at 0 and 3 hours, in wild type (JC-1687), *sae2*Δ (JC-5118), *dna2*-1 (JC-5479) and no tag control (JC-727).

(C) Enrichment of yKu70^{Myc} at DSB, at 0 and 3 hours, in wild type (JC-2271), *sae2*Δ (JC-5534), *dna2*-1 (JC-5533) and no tag control (JC-727).

(D) Enrichment of Sae2^{HA} at DSB, at 0 and 3 hours, in wild type (JC-5116), *dna2*-1 (JC-5682) and no tag control (JC-727).

(E) Enrichment of Sae2^{HA} at DSB, at 0 and 3 hours, in wild type (JC-5116), *sgs1*Δ (JC-5684), *exo1*Δ (JC-5688), *nej1*Δ (JC-5124), *sgs1*Δ *nej1*Δ (JC-5685), *exo1*Δ *nej1*Δ (JC-5686), *mre11*-3 (JC-5119), *mre11*-3 *sgs1*Δ (JC-5704), *mre11*-3 *nej1*Δ (JC-5702), *mre11*-3 *sgs1*Δ *nej1*Δ (JC-5706) and no tag control (JC-727).

All the ChIP signals were determined at 0.6kb from DSB. The fold enrichment is normalized to recovery at the SMC2 locus. For all the experiments - error bars represent the standard error of three replicates. Significance was determined using 1-tailed, unpaired Student's t test. All strains compared are marked ($P<0.05$*; $P<0.01$**; $P<0.001$***) unless specified with a line, strains are compared to WT.

Supplementary Figure S2.

Scatter data plot showing the tethering of DSB ends, at 0 and 2 hours, as measured by the distance between the GFP and mCherry foci in wild type (JC- 4066), *sgs1*Δ (JC-5699), *exo1*Δ (JC-5700) and *dna2*-1 (JC-5701). The Geometric mean (GM) distance for each sample is specified under respective sample data plot. Significance was determined using Kruskal-Wallis and Dunn's multiple comparison test.

Supplementary Figure S3.

Expression of proteins upon galactose induction. Western blots showing the expression of proteins fused to LexA and HA tag upon galactose induction. Ponceau stained membrane was used as a loading control.

Table S1 Yeast Strains: The yeast strains used in this study are outlined.

Strain	Genotype	Reference
JC-727	MAT α; *hml*::*ADE1 hmr*::*ADE1 ade3*::GAL-HO *ade1*-100 *leu*2-3, 112 *lys*5 *trp*1::*hisG ura3*-52	JKM179, [Lee et al. 1998]
JC-1280	MAT α; leu2::proLeu2-lexAop6 his3 ura3-52	Mojumdar er al. 2019
JC-1342	JC-727 with *nej1*Δ::*KanMX6*	MAV015, [Valencia et al. 2001]
JC-1687	JC-727 with *NEJ1-13MYC*::*TRP1*	Sorenson et al. 2017
JC-2271	JC-727 with *yKU70-13MYC*::*HIS3*	Sorenson et al. 2017
JC-3311	JC-1687 with *rad50*Δ::*NatRMX4*	Mojumdar er al. 2019
JC-3585	MAT a; *hml*::*ADE1 hmr*::*ADE1 ade3*::GAL-HO *ade1*-100 *leu*2-3, 112 *lys*5 *trp*1::*hisG ura3*-52	JKM179, [Lee et al. 1998]
JC-3757	JC-727 with *sgs1*Δ::*NatRMX4*	Mojumdar er al. 2019
JC-3759	JC-1342 with *sgs1*Δ::*NatRMX4*	Sorenson et al. 2017
JC-3767	JC-727 with *exo1*Δ::*NatRMX4*	Mojumdar er al. 2019
JC-3884	JC-3585 with *nej1*Δ::*KanMX6*	Sorenson et al. 2017
JC-3885	JC-3884 with *sgs1*Δ::*NatRMX4*	Mojumdar er al. 2019
JC-4066	JC-3585 with *ura3*::LacI-mCherry-*URA3*; *leu2*::TetR-GFP-*LEU2*; TAF2-LacOpFx-*TRP1*; 4.4kb MAT-TetO-*LEU2.*	Mojumdar er al. 2019
JC- 4117	JC-727 with *DNA2-6HA::TRP1*	Mojumdar er al. 2019
JC-4118	JC-4117 with *nej1*Δ::*KanMX6*	Mojumdar er al. 2019
JC-4135	JC-727 with *SGS1-6HA*::*TRP1*	Mojumdar er al. 2019
JC-4364	JC-4066 with *nej1*Δ::*KanMX6*	Mojumdar er al. 2019
JC-4556	JC-1280 with *nej1*Δ::*KanMX6*	Mojumdar er al. 2019
JC-5116	JC-727 with *SAE2-6HA*::*TRP1*	This study
JC-5118	JC-1687 with *sae2*Δ::*HIS3*	This study
JC-5119	JC-5116 with *mre11-3*::*URA3*	This study
JC-5122	JC-5116 with *mre11*Δ::*NatRMX4*	This study
JC-5123	JC-1687 with *mre11-3*::*URA3*	This study
JC-5124	JC-5116 with *nej1*Δ::*KanMX6*	This study
JC-5369	JC-1342 with *mre11-3*::*URA3*	This study
JC-5370	JC-3767 with *mre11-3*::*URA3*	This study
JC-5371	JC-5369 with *exo1*Δ::*NatRMX4*	This study
JC-5372	JC-727 with *mre11-3*::*URA3*	This study
JC-5373	JC-1342 with *exo1*Δ::*NatRMX4*	This study
JC-5405	JC-3757 with *mre11-3*::*URA3*	This study
JC-5479	JC-1687 with d*na2-1*::*TS*	This study
JC-5480	JC-5597 with *sgs1*Δ::*NatRMX4*	This study
JC-5500	JC-5369 with *sae2*Δ::*HIS3*	This study
JC-5501	JC-5372 with *sae2*Δ::*HIS3*	This study
JC-5524	JC-4066 with *sae2*Δ::*HIS3*	This study
JC-5525	JC-4364 with *sae2*Δ::*HIS3*	This study

JC-5526	JC-4364 with *mre11-3*::*URA3*	This study
JC-5529	JC-4066 with *mre11-3*::*URA3*	This study
JC-5530	JC-5524 with *mre11-3*::*URA3*	This study
JC-5531	JC-5525 with *mre11-3*::*URA3*	This study
JC-5532	JC-5670 with *mre11-3*::*URA3*	This study
JC-5533	JC-2271 with *dna2-1*::*TS*	This study
JC-5534	JC-2271 with *sae2*Δ::*HIS3*	This study
JC-5562	JC-4117 with *sae2*Δ::*HIS3*	This study
JC-5593	JC-5596 with *sae2*Δ::*HIS3*	This study
JC-5594	JC-4117 with *mre11-3*::*URA3*	This study
JC-5596	JC-4118 with *mre11-3*::*URA3*	This study
JC-5597	JC-4118 with *sae2*Δ::*HIS3*	This study
JC-5598	JC-5562 with *mre11-3*::*URA3*	This study
JC-5621	JC-5594 with *sgs1*Δ::*NatRMX4*	This study
JC-5623	JC-5596 with *sgs1*Δ::*NatRMX4*	This study
JC-5624	JC-4117 with *sgs1*Δ::*HphMX4*	This study
JC-5626	JC-4117 with *exo1*Δ::*NatRMX4*	This study
JC-5627	JC-4118 with *sgs1*Δ::*HphMX4*	This study
JC-5655	JC-727 with *dna2-1*::*TS*	This study
JC-5666	JC-4118 with *exo1*Δ::*NatRMX4*	This study
JC-5667	JC-3759 with *mre11-3*::*URA3*	This study
JC-5669	JC-5655 with *sae2*Δ::*HIS3*	This study
JC-5670	JC-5655 with *nej1*Δ::*KanMX6*	This study
JC-5671	JC-5670 with *sae2*Δ::*HIS3*	This study
JC-5673	JC-727 with *sae2*Δ::*HIS3*	This study
JC-5675	JC-1342 with *sae2*Δ::*HIS3*	This study
JC-5681	JC-4135 with *dna2-1*::*TS*	This study
JC-5682	JC-5116 with *dna2-1*::*TS*	This study
JC-5684	JC-5116 with *sgs1*Δ::*HphMX4*	This study
JC-5685	JC-5124 with *sgs1*Δ::*HphMX4*	This study
JC-5686	JC-5124 with *exo1*Δ::*NatRMX4*	This study
JC-5688	JC-5116 with *exo1*Δ::*NatRMX4*	This study
JC-5689	JC-5670 with *exo1*Δ::*NatRMX4*	This study
JC-5692	JC-5655 with *exo1*Δ::*NatRMX4*	This study
JC-5699	JC-4066 with *sgs1*Δ::*HphMX4*	This study
JC-5700	JC-4066 with *exo1*Δ::*NatRMX4*	This study
JC-5701	JC-4066 with *dna2-1*::*TS*	This study
JC-5702	JC-5119 with *nej1*Δ::*KanMX6*	This study
JC-5704	JC-5119 with *sgs1*Δ::*HphMX4*	This study
JC-5706	JC-5685 with *mre11-3*::*URA3*	This study
JC-5707	JC-727 with *dna2-1-3HA::TRP1*	This study
JC-5745	JC-5655 with *sgs1*Δ::*HphMX4*	This study
JC-5746	JC-5670 with *sgs1*Δ::*HphMX4*	This study

JC-5748	JC-5655 with *mre11-3*::*URA3*	This study
JC-5749	JC-3885 with *sae2*Δ::*HIS3*	This study
JC-5750	JC-3759 with *sae2*Δ::*HIS3*	This study

Table S2 Plasmids: Plasmids used in this study are listed below.

Plasmid number	Description
J-965	pGAL-lexA
J-1493	pJG4-6
J-359	pSH18-34 lexAGal1-lacZ
J-125	J-965 with Nej1
J-186	J-965 with Mre11
J-199	J-965 with Xrs2
J-200	J-965 with Rad50
J-1855	J-965 with Dna2-(1-440) N-term
J-1856	J-965 with Dna2-(441-920) Nuclease
J-1857	J-965 with Dna2-(921-1522) Helicase
J-1898	J-1493 with Sae2

Table S3 Primers: Table of Primers and Probes used in these studies.

Primer Name	Primer Sequence (5'-3')
HO2 Forward Primer	TTGCCCACTTCTAAGCTGATTTC
HO2 Reverse Primer	GTACTTTTCTACATTGGGAAGCAATAAA
HO2 Probe	FAM-ATGATGTCTGGGTTTTGTTTGGGATGCA-TAMRA
HO6 Forward Primer	AATATGGGACTACTTCGCGCAACA
HO6 Reverse Primer	CGTCACCACGTACTTCAGCATAA
HO6 Probe	FAM-CCTGGTTTTGGTTTTGTAGAGTGGTTGACGA-TAMRA
SMC2 Forward Primer	AATTGGATTTGGCTAAGCGTAATC
SMC2 Reverse Primer	CTCCAATGTCCCTCAAAATTTCTT
SMC2 Probe	FAM-CGACGCGAATCCATCTTCCCAAATAATT-TAMRA
MAT1 Forward Primer	CCTGGTTTTGGTTTTGTAGAGTGG
MAT1 Reverse Primer	GAGCAAGACGATGGGGAGTTTC
Pre1 Forward Primer	CCCACAAGTCCTCTGATTTACATTCG
Pre1 Reverse Primer	ATTCGATTGACAGGTGCTCCCTTTTC
Dna2_F1	GGAATTCATGCCCGGAACGCCACAGAAGAACAAGAGGTCTG
Dna2_R1320	CGGGATCCCTATATTTTTTGCGTTCCAATTTTTGG
Dna2_F1321	GGAATTCATGCTAGAGTGTATAGACGGCAAAGG
Dna2_R2760	CGGGATCCCTAGGGATTTATAAATTGTACACGACC
Dna2_F2761	GGAATTCATGGCTAAAATTGGTATCTCCGTAAAACG
Dna2_R4566	CGGGATCCTCAACTTTCATACTCTTGTAGAATTTCCTTTAT
Nej1_F1	GGAATTCATGGATTCTGAGTTGAAAGGGCAGCAGC
Nej1_R1029	CGGGATCCCTATTAGTTTTTTATTCTCACCTTTCC
Mre11_F1	GGAATTCATGGACTATCCTGATCCAGACACAATAAG

Mre11_R2076	CGGGATCCCTATTTTCTTTTCTTAGCAAGGAGACTTCCAAG
Rad50_F1	GGAATTCATGAGCGCTATCTATAAATTATCTATTCAGG
Rad50_R3936	CGGGATCCCTATCAATAAGTGACTCTGTTAATATCGACC
Xrs2_F1	GGAATTCATGTGGGTAGTACGATACCAGAATACATTGG
Xrs2_R2562	CGGGATCCCTATTATCCTTTTCTTCTTTTGAACGTAAACTTCG
Sae2_F1	GGATCCGT ATGGTGACTGGTGAAGAAAATGTGTATC
Sae2_R1038	GCGGCCGC TTAACATCTAGCATATATCTGCAATAATTTATCACTC

Table S4: Table of DSB cut efficiency.

dna2-1 cut efficiency = 93.19 avg of 3 reps; Survivor doesn't show any cut ~ -3.36 avg of 3 reps

Strain	DSB cut %	Strain	DSB cut %	Strain	DSB cut %
JC-727	94.82	JC-5500	84.44	JC-5666	81.05
JC-1342	97.02	JC-5501	98.34	JC-5667	77.28
JC-3757	81.26	JC-5532	85.59	JC-5669	94.07
JC-3759	80.62	JC-5533	84.62	JC-5670	94.19
JC-4117	80.33	JC-5534	85.59	JC-5671	94.35
JC-4118	87.05	JC-5562	81.14	JC-5673	91.31
JC-5116	85.93	JC-5593	96.33	JC-5675	88.38
JC-5118	93.52	JC-5594	98.14	JC-5681	85.28
JC-5119	92.93	JC-5596	89.02	JC-5682	83.69
JC-5122	88.73	JC-5597	87.73	JC-5689	91.79
JC-5123	92.51	JC-5598	98.53	JC-5692	90.15
JC-5124	91.53	JC-5621	90.80	JC-5702	89.97
JC-5369	78.47	JC-5623	76.04	JC-5707	92.44
JC-5372	92.50	JC-5624	97.62	JC-5745	87.13
JC-5405	94.20	JC-5626	98.24	JC-5746	82.78
JC-5479	93.01	JC-5627	85.32	JC-5748	94.97
JC-5480	91.34	JC-5655	91.89	JC-5750	99.99

Figure 1

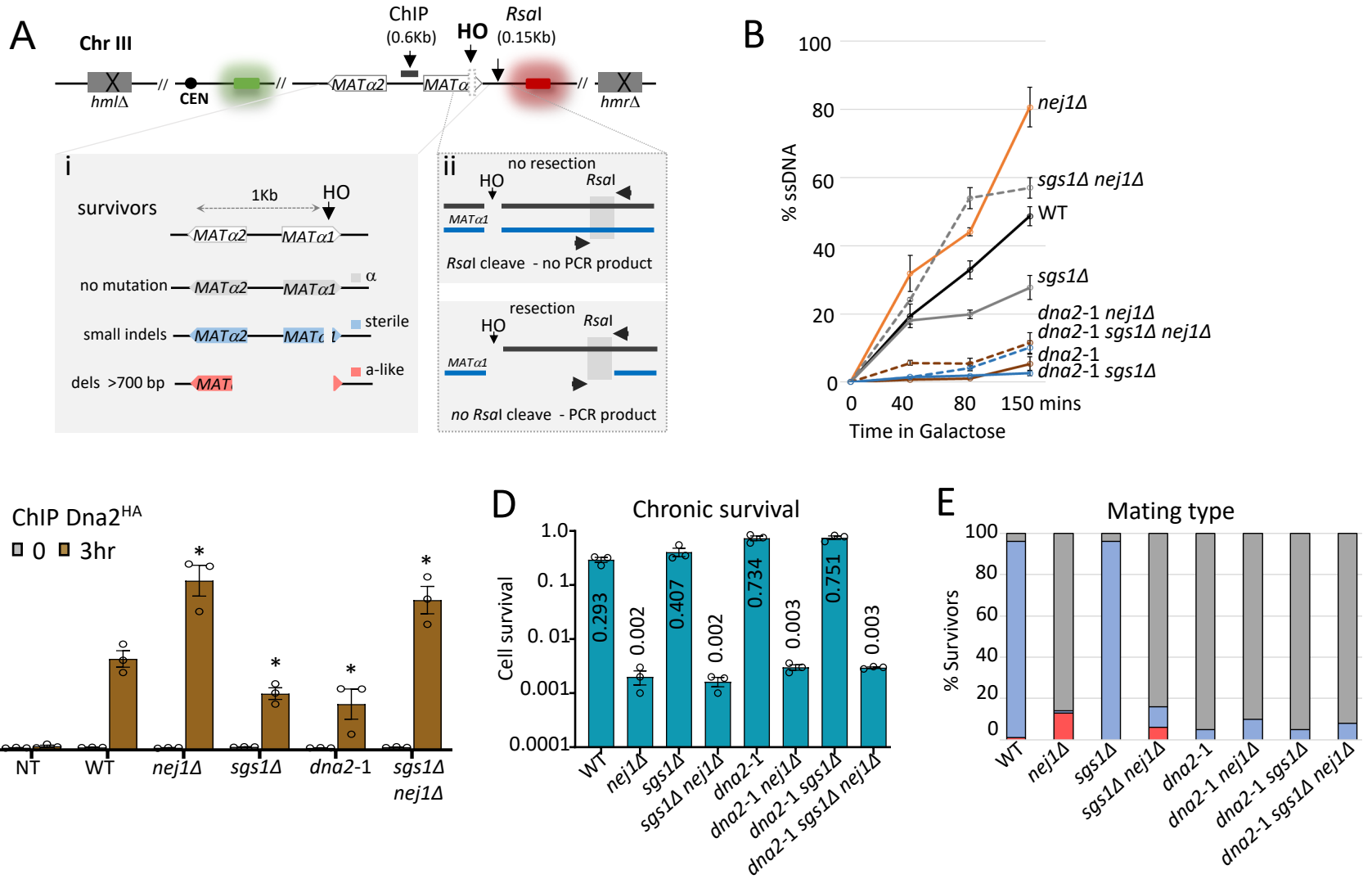
A
Chr III
hmlΔ
CEN
MATα2
MATα
ChIP
(0.6Kb)
HO
RsaI
(0.15Kb)
hmrΔ
i
survivors
1Kb
HO
MATα2
MATα1
no mutation
α
small indels
sterile
dels >700 bp
a-like
ii
no resection
HO
RsaI
MATα1
RsaI cleave - no PCR product
resection
no RsaI cleave - PCR product
B
% ssDNA
Time in Galactose
0
40
80
150 mins
nej1Δ
sgs1Δ nej1Δ
WT
sgs1Δ
dna2-1 nej1Δ
dna2-1 sgs1Δ nej1Δ
dna2-1
dna2-1 sgs1Δ
C
ChIP Dna2HA
0
3hr
Fold enrichment
NT
WT
nej1Δ
sgs1Δ
dna2-1
sgs1Δ nej1Δ
D
Chronic survival
Cell survival
0.293
0.002
0.407
0.002
0.734
0.003
0.751
0.003
WT
nej1Δ
sgs1Δ
sgs1Δ nej1Δ
dna2-1
dna2-1 nej1Δ
dna2-1 sgs1Δ
dna2-1 sgs1Δ nej1Δ
E
Mating type
% Survivors
WT
nej1Δ
sgs1Δ
sgs1Δ nej1Δ
dna2-1
dna2-1 nej1Δ
dna2-1 sgs1Δ
dna2-1 sgs1Δ nej1Δ

Figure 2

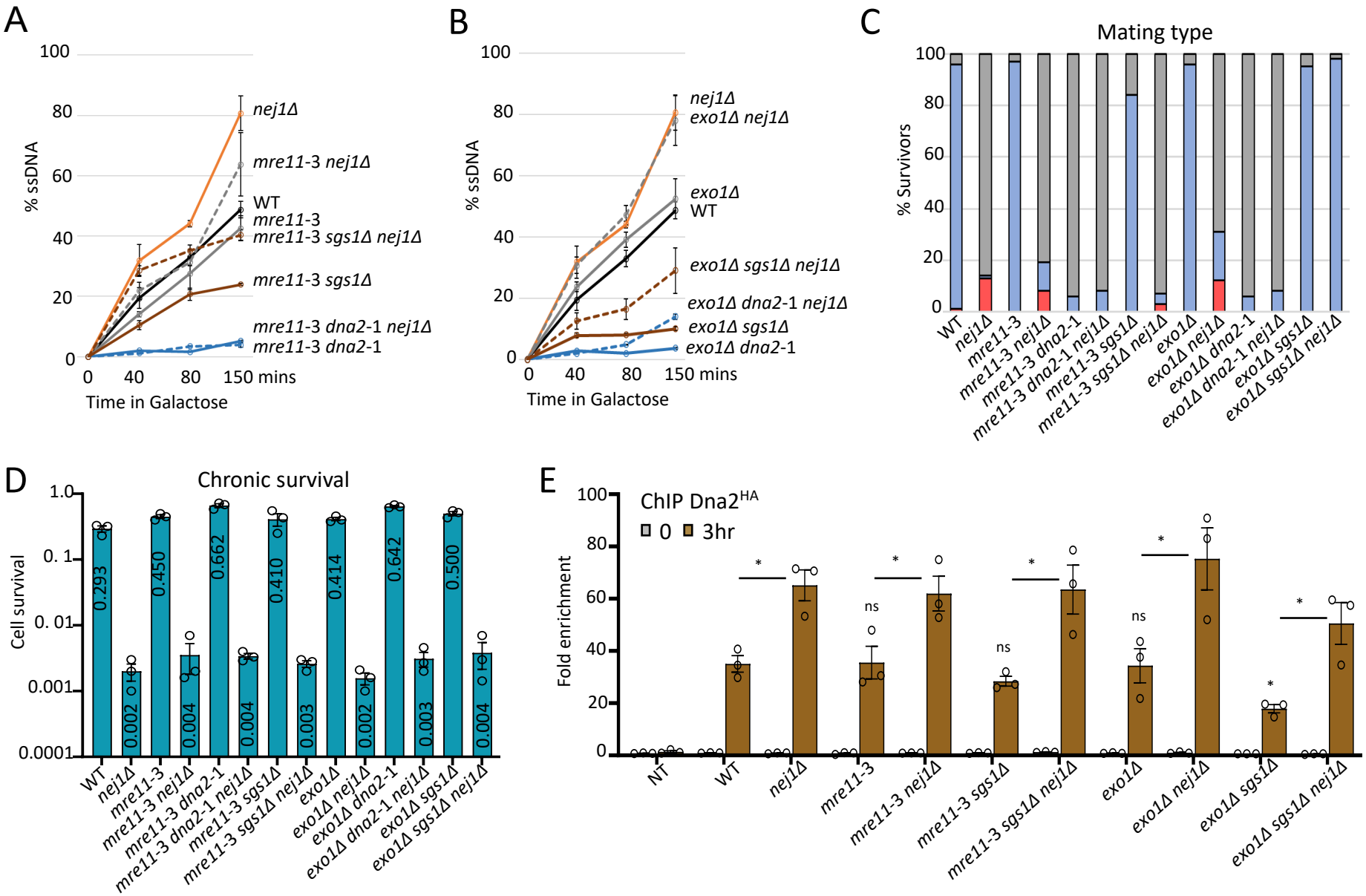
A
% ssDNA
Time in Galactose
0
40
80
150 mins
nej1Δ
mre11-3 nej1Δ
WT
mre11-3
mre11-3 sgs1Δ nej1Δ
mre11-3 sgs1Δ
mre11-3 dna2-1 nej1Δ
mre11-3 dna2-1
B
% ssDNA
Time in Galactose
nej1Δ
exo1Δ nej1Δ
exo1Δ
WT
exo1Δ sgs1Δ nej1Δ
exo1Δ dna2-1 nej1Δ
exo1Δ sgs1Δ
exo1Δ dna2-1
C
Mating type
% Survivors
WT
nej1Δ
mre11-3
mre11-3 nej1Δ
mre11-3 dna2-1
mre11-3 dna2-1 nej1Δ
mre11-3 sgs1Δ
mre11-3 sgs1Δ nej1Δ
exo1Δ
exo1Δ nej1Δ
exo1Δ dna2-1
exo1Δ dna2-1 nej1Δ
exo1Δ sgs1Δ
exo1Δ sgs1Δ nej1Δ
D
Chronic survival
Cell survival
0.293
0.002
0.450
0.004
0.662
0.004
0.410
0.003
0.414
0.002
0.642
0.003
0.500
0.004
E
ChIP Dna2HA
0
3hr
Fold enrichment
NT
ns
*

Figure 3

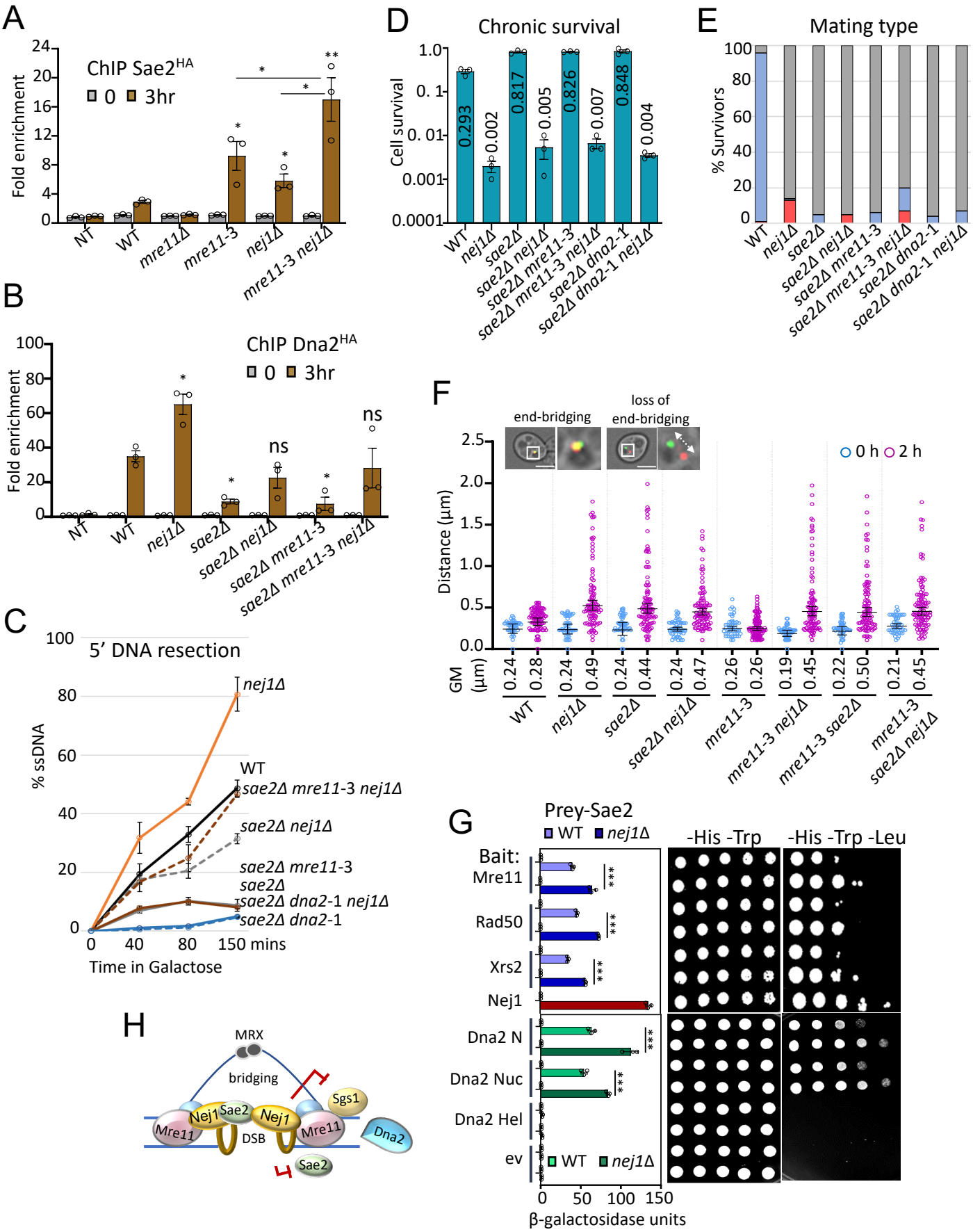
A
ChIP Sae2HA
0 3hr
Fold enrichment
NT
WT
mre11Δ
mre11-3
nej1Δ
mre11-3 nej1Δ
B
ChIP Dna2HA
0 3hr
Fold enrichment
ns
C
5' DNA resection
% ssDNA
nej1Δ
WT
sae2Δ mre11-3 nej1Δ
sae2Δ nej1Δ
sae2Δ mre11-3
sae2Δ
sae2Δ dna2-1 nej1Δ
sae2Δ dna2-1
Time in Galactose
D
Chronic survival
Cell survival
0.293
0.002
0.817
0.005
0.826
0.007
0.848
0.004
sae2Δ dna2-1
sae2Δ dna2-1 nej1Δ
E
Mating type
% Survivors
F
end-bridging
loss of end-bridging
0 h
2 h
Distance (µm)
GM (µm)
0.24 0.28
0.24 0.49
0.24 0.44
0.24 0.47
0.26 0.26
0.19 0.45
0.22 0.50
0.21 0.45
mre11-3 nej1Δ
mre11-3 sae2Δ
G
Prey-Sae2
WT nej1Δ
Bait:
Mre11
Rad50
Xrs2
Nej1
Dna2 N
Dna2 Nuc
Dna2 Hel
ev
β-galactosidase units
-His -Trp
-His -Trp -Leu
H
MRX
bridging
Sae2
Nej1
Mre11
DSB
Sgs1
Dna2

Figure 4

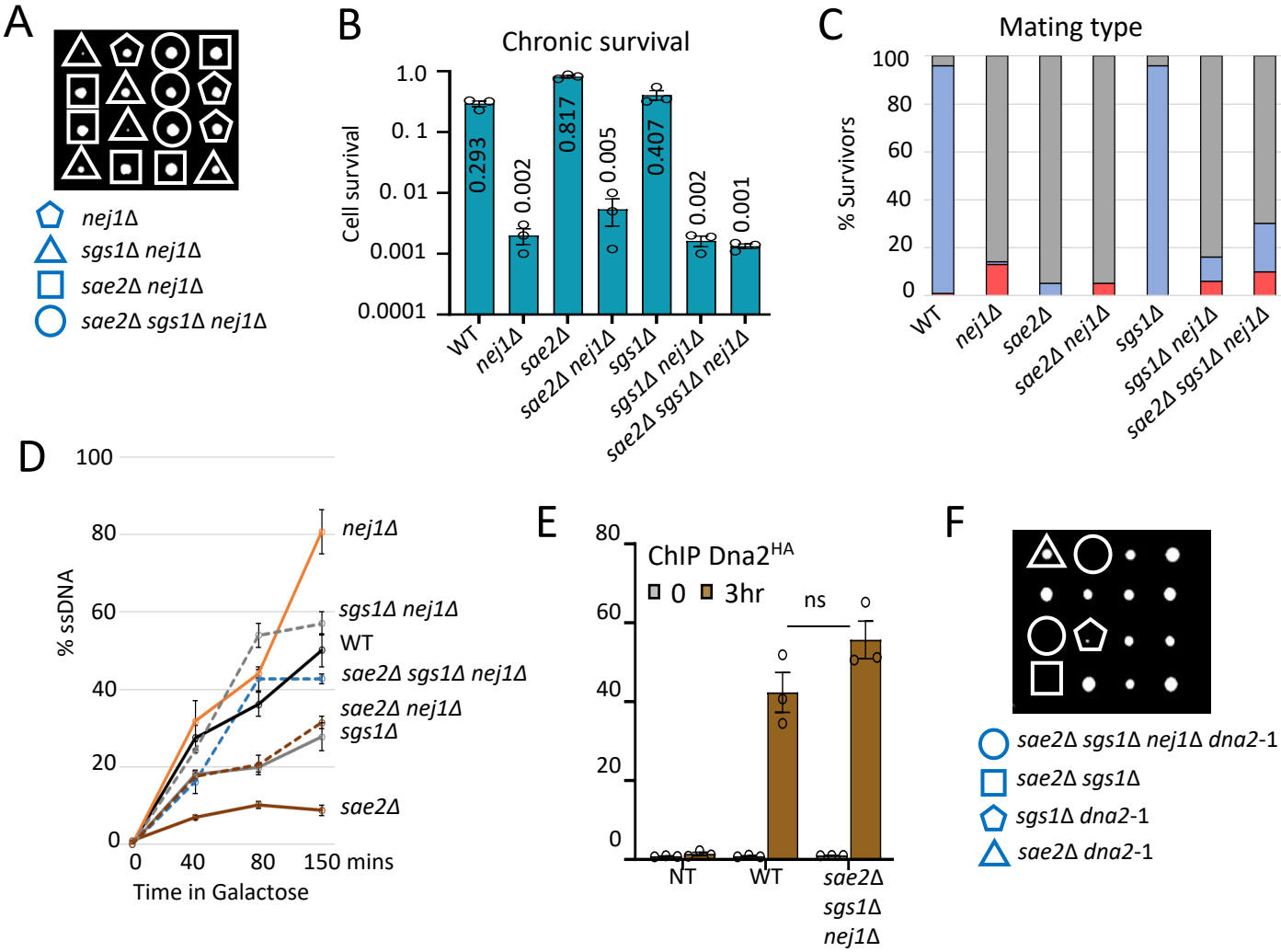
A
nej1Δ
sgs1Δ nej1Δ
sae2Δ nej1Δ
sae2Δ sgs1Δ nej1Δ
B
Chronic survival
Cell survival
1.0
0. 1
0. 01
0.001
0.0001
0.293
0.002
0.817
0.005
0.407
0.002
0.001
WT
nej1Δ
sae2Δ
sae2Δ nej1Δ
sgs1Δ
sgs1Δ nej1Δ
sae2Δ sgs1Δ nej1Δ
C
Mating type
% Survivors
100
80
60
40
20
0
WT
nej1Δ
sae2Δ
sae2Δ nej1Δ
sgs1Δ
sgs1Δ nej1Δ
sae2Δ sgs1Δ nej1Δ
D
% ssDNA
100
80
60
40
20
0
0
40
80
150 mins
Time in Galactose
nej1Δ
sgs1Δ nej1Δ
WT
sae2Δ sgs1Δ nej1Δ
sae2Δ nej1Δ
sgs1Δ
sae2Δ
E
ChIP Dna2HA
0
3hr
ns
80
60
40
20
0
NT
WT
sae2Δ
sgs1Δ
nej1Δ
F
sae2Δ sgs1Δ nej1Δ dna2-1
sae2Δ sgs1Δ
sgs1Δ dna2-1
sae2Δ dna2-1
G
Model for sae2Δ sgs1Δ lethality and rescue by NEJ1 deletion
MRX
Mre11
DSB
Nej1
Dna2
Exo1
nej1Δ
MRX
Mre11
Dna2
Exo1
5′
3′
3′
5′